Available online at www.sciencedirect.com

SciVerse ScienceDirect

Ceramics International 38 (2012) 3801–3806

CERAMICS INTERNATIONAL

www.elsevier.com/locate/ceramint

Comparison of the structural and magnetic properties of submicron barium hexaferrite powders prepared by molten salt and solid state calcination routes

Sinan Dursun [a], Ramazan Topkaya [b,c], Numan Akdoğan [b,c], Sedat Alkoy [a,*]

[a] Department of Materials Science and Engineering, Gebze Institute of Technology, 41400 Kocaeli, Turkey
[b] Department of Physics, Gebze Institute of Technology, 41400 Kocaeli, Turkey
[c] Nanomagnetism and Spintronics Research Center (NASAM), Gebze Institute of Technology, 41400 Kocaeli, Turkey

Received 12 August 2011; received in revised form 4 January 2012; accepted 9 January 2012
Available online 18 January 2012

Abstract

The effect of crystallinity and particle morphology of the submicron barium hexaferrite ($BaFe_{12}O_{19}$) powders on the magnetic properties was investigated on powders synthesized by solid-state calcination (BHF-c) and molten salt synthesis (BHF-m) methods. Solid-state calcination route was found to yield agglomerated powders with poor crystallinity, whereas molten salt synthesis resulted in well crystallized powders with an anisometric morphology. The saturation magnetization of the BHF-m and BHF-c samples is 59 emu/g, and 56 emu/g at 300 K, and 90 emu/g, and 86 emu/g at 10 K. The temperature dependence of magnetization of the BHF-m is higher and the increase in magnetocrystal anisotropy with decreasing temperature is also steeper than that of the BHF-c due to the higher crystallinity. The magnetocrystalline anisotropy constant, K, calculated from the Stoner–Wohlfarth theory, of the BHF-m and BHF-c powders is 14.24 and 10.14 HA^2/kg, respectively. The higher effective anisotropy, K_{eff} of the BHF-m is also confirmed through ferromagnetic resonance measurements. In conclusion, the higher crystallinity, slightly higher particle size and anisometric morphology of the BHF-m particles translated into higher magnetic properties and magnetocrystalline anisotropy.

Keywords: A. Powders: solid state reaction; C. Magnetic properties; D. Ferrites; Magnetocrystalline anisotropy

1. Introduction

Barium hexaferrite ($BaFe_{12}O_{19}$, BHF) also known as barium ferrite is widely used in permanent magnets [1]. It has a high Curie temperature, a large saturation magnetization, an excellent chemical stability and corrosion resistance, and it is relatively cheap to produce. Barium ferrite and its derivatives have also been used as chip inductors, and microwave absorbers in the GHz range, because they have greater permeability and higher magnetic resonance frequency than spinel ferrites [2]. But mainly, it is an important magnetic recording material. The main features that make it attractive for recording media are: (i) the anisometric particle morphology and related large magneto-crystalline anisotropy with easy magnetization axis normal to the hexagonal basal plane; (ii) the square shape of hysteresis loop; (iii) its large coercivity. However, for these applications, the ferrite should consist of uniform and fine (submicrometer) grains to allow for both a relatively large remanent magnetization and a high coercive field [3]. The magnetic recording media also require high coercivity since keeping the recorded information for a considerable time requires a high magnetic permanence.

Various methods have been used to synthesize fine $BaFe_{12}O_{19}$ powders such as: conventional solid-state calcination route [4], citrate precursor [5], chemical co-precipitation [6], hydrothermal synthesis [7], sol–gel process [8,9], crystallization from a glass precursor [10], oxidation of a metallic barium–iron precursor [11], spray pyrolysis [12] and molten salt synthesis [13] methods resulting in various particle sizes, morphologies and related magnetic properties. The composition of the ferrite is not the only parameter in the properties. The morphology of the powder particles are also reported to be influential on the magnetic properties of the ferrite powders due to the variations in the morphological anisotropy [9].

* Corresponding author. Tel.: +90 262 605 2639; fax: +90 262 653 0675.
E-mail addresses: sedal@gyte.edu.tr, sedatalkoy@gmail.com (S. Alkoy).

0272-8842/$36.00
doi:10.1016/j.ceramint.2012.01.028

Thus, in our study, $BaFe_{12}O_{19}$ powders with submicron particle sizes were synthesized by solid-state calcination and molten salt synthesis methods, and the structural and magnetic features of the particles obtained through these two methods were compared and discussed from the aspects of crystallinity and particle morphology. Solid-state calcination was chosen because this method is simpler, straightforward and less expensive compared to other synthesis methods. On the other hand, molten salt synthesis was chosen based on the fact that it allows preparation of complex oxide powders with a high shape anisotropy, i.e. anisometric morphology [13,14] and further allows the fabrication of bulk materials with crystallographically textured microstructures [15–17].

2. Material and methods

In our study, $BaFe_{12}O_{19}$ powders with submicron particle sizes were synthesized by solid-state calcination and molten salt synthesis methods. For the solid-state calcination method, a stoichiometric mixture of $BaCO_3$ (Alfa Aesar, 99.5%), Fe_2O_3 (Alfa Aesar, 99.5%) were ball milled for 24 h in isopropanol using zirconia balls in high density polyethylene bottle. Isopropanol was evaporated during fast stirring to eliminate differential powder settling. The powder mixture was put inside an alumina crucible and then calcined at 1100 °C for 6 h to synthesize single phase $BaFe_{12}O_{19}$. After calcination, powders were again ball-milled for 24 h to reduce particle size using ZrO_2 balls in isopropyl alcohol and then dried at 50 °C.

Various salts can be used in the molten salt synthesis of anisometric ferrite particles such as NaCl–KCI [13], Na_2SO_4–K_2SO_4 [18] and Na_2SO_4–Li_2SO_4 [19]. In our case $BaFe_{12}O_{19}$ particles were synthesized by reacting KCl salt with $BaFe_{12}O_{19}$ powder at a weight ratio of 2:1. The $BaFe_{12}O_{19}$ and KCl were initially mixed in an agate mortar and pestle for 1 h. Then powders were placed in covered alumina crucibles and heated up to 1150 °C at a rate of 5 °C/min., held at this temperature for 8 h and then cooled slowly to room temperature at a rate of 2 °C/min. Afterwards, the $BaFe_{12}O_{19}$ particles were washed with hot deionized water to remove salt and sonicated for 10 min. to deagglomerate particles. The samples which are prepared with molten salt and solid state calcination methods will be referred to in the text as BHF-m, and BHF-c, respectively.

The structural properties of the powders were investigated by scanning electron microscopy (SEM) (Philips XL30) and X-ray diffraction (XRD) (Rigaku Dmax 2200). The ferromagnetic resonance measurements were carried out by using Bruker EMX (9.8 GHz) ESR spectrometer. The magnetic hysteresis curves were recorded by vibrating sample magnetometer (VSM) (Quantum Design PPMS 9T) between ±30 kOe and in the temperature range of 10–400 K.

3. Results and discussion

3.1. Structural and morphological features

Results of the phase analysis of the $BaFe_{12}O_{19}$ particles by X-ray diffraction is given in Fig. 1. From this figure the main phase

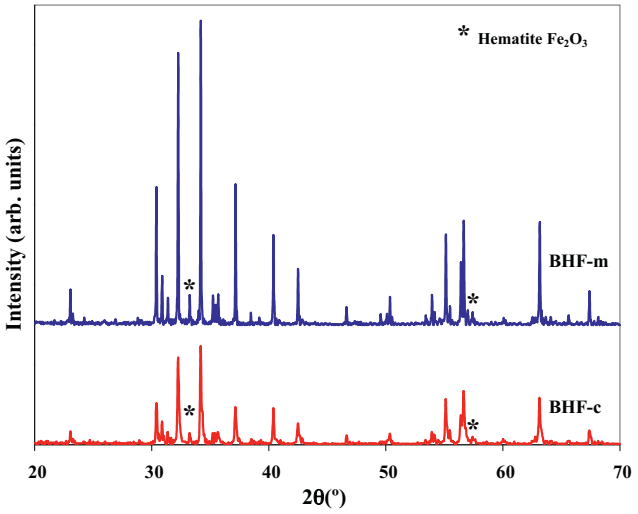

Fig. 1. X-ray diffraction patterns of $BaFe_{12}O_{19}$ particles synthesized through solid state calcinations (BHF-c) and molten salt synthesis (BHF-m) methods.

is $BaFe_{12}O_{19}$, although the peaks appeared at 33.2° and 57.4° indicated a very limited presence of α-Fe_2O_3. This is believed to be a residual phase left over from the formation of the barium hexaferrite phase due to insufficient reaction temperature and time [20]. Molten salt synthesis was found to yield a higher crystallinity, as indicated by the higher intensity of the peaks compared to the lower intensity and broadened peaks of the solid state calcination method [21]. The broadening of the peaks also indicates a lower crystallite size for the BHF-c particles synthesized with the solid state calcination route.

Morphology and size of the $BaFe_{12}O_{19}$ particles synthesized through two different methods were investigated by scanning electron microscopy and by particle size measurements. The measurement results indicate smaller particle size for BHF-c but agglomeration, nevertheless, in both cases. The micrographs obtained from SEM examination are presented in Fig. 2. The size of the BHF-c particles synthesized by SSC method, shown in Fig. 2(a), and BHF-m particles synthesized by MSS method, shown in Fig. 2(b), indicated that both of the synthesis routes led to a particle size smaller than 1 μm in largest dimension. However, at a closer look on the particle morphology at higher magnifications, it is clear that SSC method led to poorly crystallized particles with cracks and agglomeration (Fig. 2(c)), whereas molten salt synthesis resulted in a lower agglomeration and a better anisometric morphology, as seen in Fig. 2(d). The hexagonal plate-like morphology is more apparent and cracks have not been observed in this case. This is due to the more homogeneous nature of the reaction mixture and also to the efficiency of the mass transfer in the liquid medium of the molten salt synthesis approach. The diffusion distances in the intimate mix of the constituent oxides in the molten salt method is much smaller and the mobility of species in the molten salt is much higher compared with the solid state calcination routes [22]. Thus, complete reaction is accomplished in a relatively short time and a perfectly crystalline phase with shape anisotropy can be obtained with this method.

These structural differences in crystallinity and particle morphology was found to have an impact on the magnetic

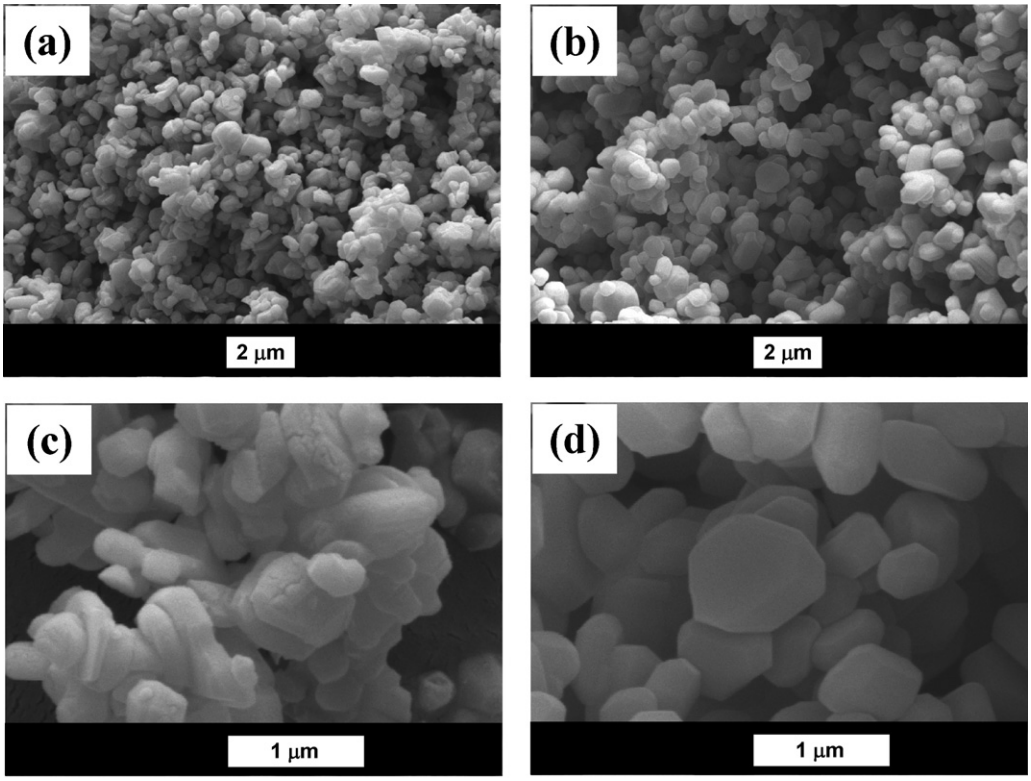

Fig. 2. Particle size and morphology of $BaFe_{12}O_{19}$ particles synthesized through (a), (c) solid state calcination route, and (b), (d) molten salt synthesis method.

properties of the particles. This effect is the main focus of our study and is discussed in details in the following section.

3.2. Magnetic properties

Magnetization curves taken at (a) 300 K and (b) 10 K for the $BaFe_{12}O_{19}$ powders prepared with two different methods are plotted in Fig. 3. As seen as from this figure, the samples exhibit a clear hysteretic behavior for the magnetization under applied magnetic field. The samples saturate at about 30 kOe and show large coercive field. The saturation magnetization (M_s) and the coercive field (H_c) of the BHF-m and BHF-c samples are given Table 1. The measured saturation magnetization and coercive field are lower than the theoretical values for single crystals of barium hexaferrites (M_s = 72 emu/g and H_c = 6700 Oe) [23]. The α-Fe_2O_3, whose presence was observed in the XRD analysis (Fig. 1), is a non-magnetic intermediate phase. Interaction between non-magnetic and magnetic particles affects the magnetic anisotropy and therefore changes magnetic properties of the samples [24]. This is believed to be why the saturation magnetization and coercive field is lower than the theoretical values. Also the saturation magnetization of the BHF-m is higher than that of the BHF-c due to the higher crystallite/particle size, better crystallinity and anisometric morphology of the BHF-m compared to the BHF-c. Similar results were also obtained by Kim et al. [25] in their study on Sr-ferrite ($SrFe_{12}O_{19}$) powders.

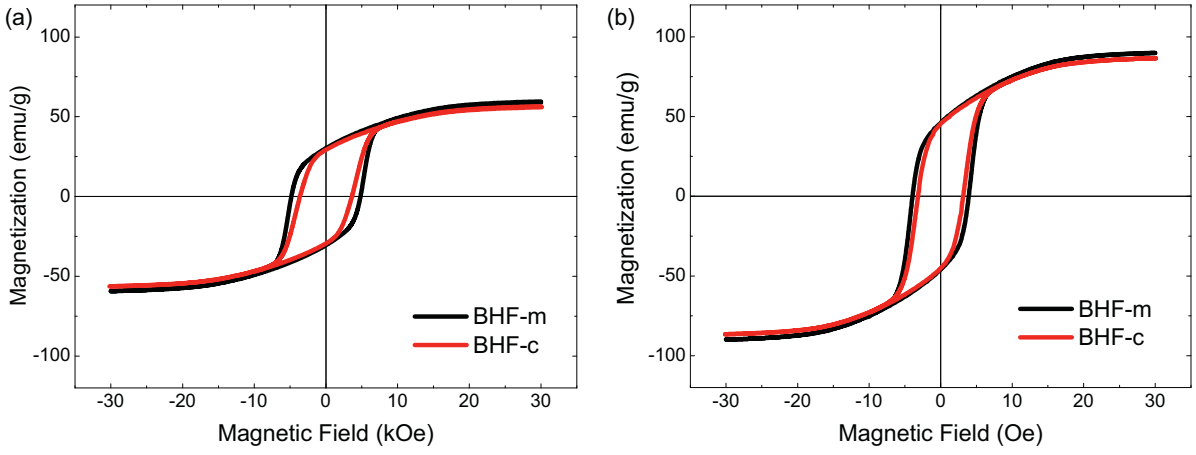

Fig. 3. Magnetization curves for the $BaFe_{12}O_{19}$ powders measured at (a) 300 K and (b) 10 K using VSM.

Table 1
Magnetic properties of powders synthesized with two different methods.

Synthesis method	Coercive field H_c (kOe) @10 K	Saturation magnetization M_s (emu/g) @10 K	Coercive field H_c (kOe) @300 K	Saturation magnetization M_s (emu/g) @300 K	Magnetocrystalline anisotropy constant K (HA^2/kg)	The line width of resonance (kOe)
Solid state calcination (BHF-C)	3.14	86	3.62	56	10.14	2.1
Molten salt synthesis (BHF-M)	3.94	90	4.82	59	14.24	1.6

Fig. 3 also indicates that the coercive field of the BHF-m is higher than that of the BHF-c due to the higher magnetocrystalline anisotropy of the BHF-m, which in turn is due to the anisometric morphology of the particles synthesized with this method. Because, the coercive field (H_c) of a magnetic material is a measure of its magnetocrystalline anisotropy [26,27].

According to Stoner–Wohlfarth theory [28], the coercivity of nanoparticles is determined by the magnetocrystalline anisotropy constant (K) and saturation magnetization (M_s):

$$H_c = \frac{2K}{\mu_0 M_s} \quad (1)$$

where μ_0 is the universal constant of permeability in free space, $4\pi \times 10^{-7}$ H/m. Since M_s and H_c are determined from VSM measurements, the magnetocrystalline anisotropy constant (K) can be calculated using this equation. In our case, the calculated magnetocrystalline anisotropy constant of the BHF-m and BHF-c powders are given in Table 1 as 14.24 and 10.14 HA^2/kg, respectively. This result also supports our claim that BHF-m has better crystallinity than that of the BHF-c.

In order to investigate the temperature dependence of magnetization, we have carried out field cooled (FC) M–T measurements. Fig. 4 presents M–T data of the BHF-m and BHF-c samples. For field cooled M–T measurements the applied field of 50 Oe is kept constant during cooling from 400 K down to 10 K and the magnetization is recorded during field warming within the same field value. When the temperature is increased, magnetization decreases in both samples as it is expected due to the thermal agitations which fights against the magnetic order. This decrease in magnetization is much faster for BHF-m sample. However, even at 400 K BHF-m sample has much bigger magnetization compared to the NHF-c sample. This is in agreement with the structural results which claims that the BHF-m sample has better crystalline structure.

For further investigation of magnetic properties, the ferromagnetic resonance measurements were performed at X-Band (9.8 GHz) frequency. In order to do FMR experiments the powders were prepared as pellet film. A goniometer was used to rotate the sample holder which is parallel to the microwave magnetic field and perpendicular to the applied static magnetic field. The sample was replaced on a sample holder in two different geometries. For the in-plane geometry the sample was attached horizontally at bottom edge (horizontal surface) of sample holder. During in-plane rotations, the film normal kept parallel to the microwave magnetic field, but external dc magnetic field was aligned at different orientation with respect to the sample axis. At out-of-plane geometry the sample was attached to the flat platform of sample holder where the magnetic field of microwave lie in film plane and static magnetic field is rotated from the sample plane to the film normal. At in-plane geometry the resonance lines are not angular dependent. This means that the external

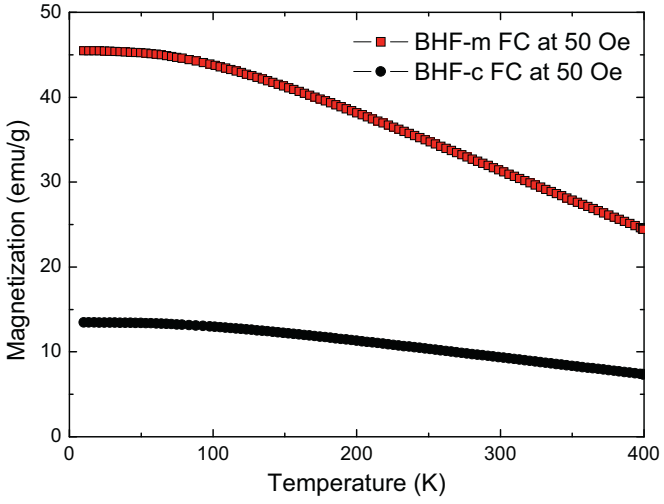

Fig. 4. Magnetization vs. temperature curves of the BHF-m and BHF-c samples taken under an applied magnetic field of 50 Oe.

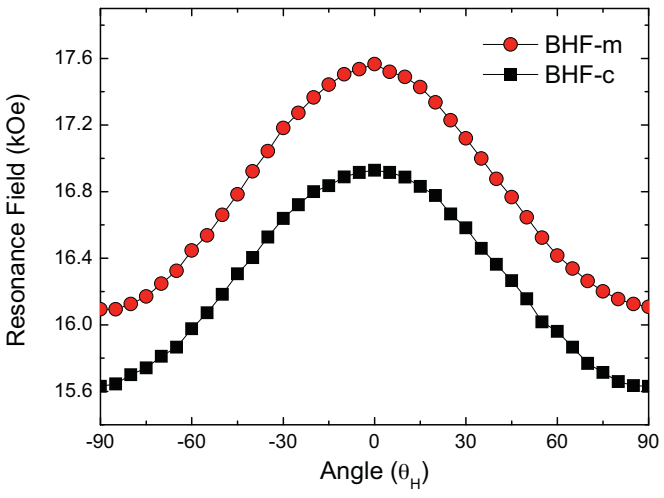

Fig. 5. Angular dependence of the FMR resonance field of the samples in the out-of-plane geometry.

field did not re-orient the particle axes along the field directions. The line width of the resonance lines, as given in Table 1, are about 1.6 kOe for the BHF-m and about 2.1 kOe for the BHF-c. This broad line seems to be originated from different resonance fields of randomly distributed particles which have different orientation of magnetic easy axes. As seen from Figs. 1 and 2, the particle size, crystallinity and anisometric morphology of the BHF-m sample is higher than that of the BHF-c sample. Thus, the line width of resonance spectrum of the BHF-c is larger than that of BHF-m. The angular dependence of FMR signal of the samples in the out-of-plane geometry is presented in Fig. 5. Fig. 5 clearly shows that the out-of-plane resonance field values of the BHF-m are higher than that of the BHF-c for all directions of the field. It means that the effective anisotropy, K_{eff} of the BHF-m is higher than that of BHF-c. This is another result of better crystallinity of BHF-m sample and confirms the calculations done by Eq. (1).

4. Conclusions

This study was conducted to investigate the effect of crystallinity and particle morphology of the submicron $BaFe_{12}O_{19}$ powders on the magnetic properties. Particles with submicron sizes and within similar size range were synthesized by solid-state calcination (BHF-c) and molten salt synthesis (BHF-m) methods. Solid-state calcination route yielded agglomerated powders with poor crystallinity, whereas molten salt synthesis resulted in well crystallized powders with a high shape anisotropy, i.e. anisometric morphology. Both of the particles contained a limited presence of α-Fe_2O_3 as a secondary phase. These structural differences in crystallinity and particle morphology were found to have an impact on the magnetic properties of the particles.

The saturation magnetization of the BHF-m and BHF-c samples is 59 emu/g, and 56 emu/g at 300 K, and 90 emu/g, and 86 emu/g at 10 K. Values are higher for BHF-m due to the higher crystallite/particle size, better crystallinity and anisometric morphology of the BHF-m compared to the BHF-c. The magnetocrystalline anisotropy constant, K, was calculated from the Stoner–Wohlfarth theory using measured M_s and H_c data obtained from VSM measurements. The calculated K constant of the BHF-m and BHF-c powders is 14.24 and 10.14 HA^2/kg, respectively. The higher effective anisotropy, K_{eff} of the BHF-m is also confirmed through ferromagnetic resonance measurements. In conclusion, the higher crystallinity, slightly higher particle size and anisometric morphology of the BHF-m particles translated into higher magnetic properties and magnetocrystalline anisotropy.

References

[1] R.M. Almeida, W. Paraguassu, D.S. Pires, R.R. Corrêa, C.W.A. Paschoal, Impedance spectroscopy analysis of $BaFe_{12}O_{19}$ M-type hexaferrite obtained by ceramic method, Ceramics International 35 (2009) 2443–2447.

[2] Y. Liu, M.G.B. Drew, Y. Liu, J. Wang, M. Zhang, Preparation characterization and magnetic properties of the doped barium hexaferrites $BaFe_{12-2x}Co_{x/2}Zn_{x/2}Sn_xO_{19}$, $x = 0.0–2.0$, Journal of Magnetism and Magnetic Materials 322 (2010) 814–818.

[3] B.T. Shirk, W.R. Buessem, Theoretical experimental aspects of coercivity versus particle size for barium ferrite, IEEE Transactions on Magnetics 3 (1971) 659–663.

[4] M. Gadalla, H.W. Hennicke, Formation of barium hexaferrite, Journal of Magnetism and Magnetic Materials 1 (2) (1975) 144–152.

[5] M.C. Dimri, S.C. Kashyap, D.C. Dube, Electrical and magnetic properties of barium hexaferrite nanoparticles prepared by citrate precursor method, Ceramics International 30 (2004) 1623–1626.

[6] W. Roos, Formation of chemically coprecipitated barium ferrite, Journal of the American Ceramic Society 63 (11) (1980) 601–603.

[7] D. Barb, L. Diamandescu, A. Rusi, D. Tarabasanu-Mihaila, M. Morariu, V. Teodorescu, Preparation of barium hexaferrite by a hydrothermal method: structure and magnetic properties, Journal of Materials Science 21 (1986) 1118–1122.

[8] K. Oda, T. Yoshio, K. Hirata, K. O-Oka, K. Takahashi, Preparation of barium ferrites from metal alkoxides, Journal of the Japan of Society of Powder and Powder Metallurgy 29 (5) (1982) 170–175.

[9] S. Singhal, T. Namgyal, J. Singh, K. Chandra, S. Bansal, A comparative study on the magnetic properties of MFe12O19 and MAlFe11O19 (M = Sr, Ba and Pb) hexaferrites with different morphologies, Ceramics International 37 (2011) 1833–1837.

[10] B.T. Shirk, W.R. Buessem, Magnetic properties of barium ferrite formed by crystallization of a glass, Journal of the American Ceramic Society 53 (4) (1970) 192–196.

[11] G.A. Ward, K.H. Sandhage, Synthesis of barium hexaferrite by the oxidation of a metallic barium–iron precursor, Journal of the American Ceramic Society 80 (6) (1997) 1508–1516.

[12] M.H. Kim, D.S. Jung, Y.C. Kang, J.H. Choi, Nanosized barium ferrite powders prepared by spray pyrolysis from citric acid solution, Ceramics International 35 (2009) 1933–1937.

[13] R.H. Arendt, The molten salt synthesis of single magnetic domain $BaFe_{12}O_{19}$ and $SrFe_{12}O_{19}$ crystals, Journal of Solid State Chemistry 8 (1973) 339–347.

[14] C. Duran, G.L. Messing, S. Trolier-McKinstry, Molten salt synthesis of anisometric particles in the SrO–Nb_2O_5–BaO system, Materials Research Bulletin 39 (2004) 1679–1689.

[15] D.B. Hovis, K.T. Faber, Textured microstructures in barium hexaferrite by magnetic field assisted gelcasting and templated grain growth, Scripta Materialia 44 (2001) 2525–2529.

[16] S. Alkoy, C. Duran, D.A. Hall, Electrical properties of textured potassium strontium niobate ($KSr_2Nb_5O_{15}$) ceramics fabricated by reactive templated grain growth, Journal of the American Ceramic Society 91 (5) (2008) 1597–1602.

[17] S. Alkoy, M.Y. Kaya, N. Akdoğan, Proc. 7th International Workshop on Piezoelectric Materials and Applications in Actuators, Antalya, Turkey, October 10–13, (2010), p. 11.

[18] K.H. Yoon, D.H. Lee, H.J. Jung, S.O. Yoon, Molten salt synthesis of anisotropic $BaFe_{12}O_{19}$ powders, Journal of Materials Science 27 (1992) 2941–2945.

[19] H.I. Hsiang, C.H. Chang, Molten salt synthesis and magnetic properties of $3BaO{\cdot}2CoO{\cdot}12Fe_2O_3$ powder, Journal of Magnetism and Magnetic Materials 278 (2004) 218–222.

[20] Y. Liu, M.G.B. Drew, Y. Liu, J. Wang, M. Zhang, Preparation and magnetic properties of La–Mn and La–Co doped barium hexaferrites prepared via an improved co-precipitation/molten salt method, Journal of Magnetism and Magnetic Materials 322 (2010) 3342–3345.

[21] T. Mochiku, K. Hirata, K. Kadowaki, Crystallinity improvement of $Bi_2Sr_2CaCu_2O_{8+\delta}$ single crystal by TSFZ method, Physica C 282 (287) (1997) 475–476.

[22] R.H. Arendt, J.H. Rosolowski, J.W. Szymaszek, Lead zirconate titanate ceramics from molten salt solvent synthesized powders, Materials Research Bulletin 14 (5) (1979) 703–709.

[23] B.T. Shirk, W.R. Buessem, Temperature dependence of M_s and K_1 of $BaFe_{12}O_{19}$ and $SrFe_{12}O_{19}$ single crystals, Journal of Applied Physics 40 (1969) 1294.

[24] C.R. Vestal, Q. Song, Z.J. Zhang, Effects of interparticle interactions upon the magnetic properties of $CoFe_2O_4$ and $MnFe_2O_4$ nanocrystals, Journal of Physical Chemistry B 108 (2004) 18222.

[25] S.D. Kim, J.S. Kim, Magnetic properties of Sr-ferrites synthesized in molten (NaCl + KCl) flux, Journal of Magnetism and Magnetic Materials 307 (2006) 295–300.

[26] X. Huang, Z. Chen, Nickel ferrite on silica nanocomposites prepared by the sol–gel method, Journal of Magnetism and Magnetic Materials 280 (1) (2004) 37–43.

[27] H. Kavas, A. Baykal, M.S. Toprak, Y. Koseoğlu, M. Sertkol, B. Aktaş, Cation distribution and magnetic properties of Zn doped $NiFe_2O_4$ nanoparticles synthesized by PEG-assisted hydrothermal route, Journal of Alloys and Compounds 479 (2009) 49–55.

[28] E.C. Stoner, E.P. Wohlfarth, A mechanism of magnetic hysteresis in heterogeneous alloys, IEEE Transactions on Magnetics 27 (4) (1991) 3475–3518.